LETTERS

An excess of cosmic ray electrons at energies of 300–800 GeV

J. Chang[1,2], J. H. Adams Jr[3], H. S. Ahn[4], G. L. Bashindzhagyan[5], M. Christl[3], O. Ganel[4], T. G. Guzik[6], J. Isbert[6], K. C. Kim[4], E. N. Kuznetsov[5], M. I. Panasyuk[5], A. D. Panov[5], W. K. H. Schmidt[2], E. S. Seo[4], N. V. Sokolskaya[5], J. W. Watts[3], J. P. Wefel[6], J. Wu[4] & V. I. Zatsepin[5]

Galactic cosmic rays consist of protons, electrons and ions, most of which are believed to be accelerated to relativistic speeds in supernova remnants[1–3]. All components of the cosmic rays show an intensity that decreases as a power law with increasing energy (for example as $E^{-2.7}$). Electrons in particular lose energy rapidly through synchrotron and inverse Compton processes, resulting in a relatively short lifetime (about 10^5 years) and a rapidly falling intensity, which raises the possibility of seeing the contribution from individual nearby sources (less than one kiloparsec away)[4]. Here we report an excess of galactic cosmic-ray electrons at energies of ~300–800 GeV, which indicates a nearby source of energetic electrons. Such a source could be an unseen astrophysical object (such as a pulsar[5] or micro-quasar[6]) that accelerates electrons to those energies, or the electrons could arise from the annihilation of dark matter particles (such as a Kaluza–Klein particle[7] with a mass of about 620 GeV).

High-energy electrons are rare. Before now, only emulsion chamber data have been available (above 10^{11} eV)[4,8], and these were of limited resolution, owing to the small depth of the calorimeters used, and low statistical significance, as the results were analysed manually[9]. Here we present new data from the Advanced Thin Ionization Calorimeter (ATIC) instrument[10,11], which contains a deep, fully active, bismuth germanate (BGO) calorimeter of 18 radiation lengths (X_o, a characteristic distance for energy loss by bremsstrahlung) in eight layers arranged in orthogonal pairs to measure the energy deposited through a cascade (shower) of nuclear and electromagnetic interactions. At each step of the cascade, the energy of the primary particle is subdivided among many secondary particles. The area under the curve of ionization energy plotted against depth in the medium provides a measure of the incident particle energy, and the lateral distribution of energy across each layer can be used to separate electrons from protons. The topmost element is a pixelated silicon matrix (SiM) detector (4,480 pixels) which measures the charge of the incident particle. This is followed by three layers of scintillator hodoscopes embedded within a 30-cm-thick graphite target (this amount of material is 0.75 times the proton interaction length, and 1.5 times X_o). We determine the trajectory by using the hodoscopes along with cascade centroid positions in the BGO calorimeter.

The ATIC instrument has been studied extensively with GEANT and FLUKA simulations and was calibrated at the CERN SPS with proton and electron beams[11]. The accelerator data validated the simulations, demonstrated an electron energy resolution of around 2% and verified the hadron–lepton separation capabilities[11,12]. The detailed electron data analysis is described elsewhere[12,13], and is reviewed briefly here and in the Supplementary Information (section 1). The basic ATIC energy calibration is provided by cosmic-ray muons recorded just before each flight, as well as by the shower data itself. The raw flight data are processed to physics units using these calibrations plus the temperature dependence of the BGO response.

The trajectory of each event is extrapolated to the SiM and identifies the pixels containing the primary particle signal. The SiM separates events with atomic number $Z \geq 2$ from the $Z = 0$, 1 events, and an absence of signal indicates a γ-ray candidate. The cascade profile is then analysed in the calorimeter. Electromagnetic cascades from electrons and γ-rays are narrower than hadronic cascades induced by interacting protons (whose products spread throughout the 30-cm target region). In addition, electrons and γ-rays deposit at least 85% of their energy in the calorimeter, whereas hadronic events deposit around 35%. Thus, at the bottom of the calorimeter the electron showers are dying out, whereas hadronic showers are usually still developing. As illustrated in Fig. 1, for electron candidates with energies over 50 GeV, in the histogram of Fig. 1, the electron peak (left of figure) is separated from the protons. Moreover, the atmospheric secondary γ-rays provide a calibration for the electron–proton separation (see Supplementary Information section 1 for details.)

For consistency checking, the data were analysed (1) in different zenith angle bins, (2) in different time periods corresponding to different trigger conditions, (3) in different physical sections of the apparatus and (4) with more severe geometrical cuts on the SiM and the calorimeter edge crystals. Furthermore, we carried out a 'blind' study in which all events were subject to the electron analysis. After correcting for the known differences in $Z \geq 2$ showers compared with protons, this analysis verified the electron–proton separation[12] (Supplementary Information section 2). A convolution of the rejection function with the measured proton energy deposit spectra provides the (energy-dependent) proton background. In Fig. 2 we show the raw spectrum of electron candidates at the instrument (multiplied by E^3, where E is electron energy) for both the ATIC-1 and ATIC-2 flights, which are in excellent agreement. We also show the combined background (unresolved protons, misidentified γ-rays and atmospheric secondary electrons), which must be subtracted from the raw data.

After subtracting the background from each energy bin and correcting for energy loss in the overlying atmosphere, the absolute primary electron spectrum at the top of atmosphere is obtained (Fig. 3). Below 100 GeV, the ATIC spectrum agrees with previous data and with the 'general' spectrum calculated with the GALPROP interstellar propagation code[14]. Above about 100 GeV, the results

[1]Purple Mountain Observatory, CAS, 2 West Beijing Road, Nanjing 210008, China. [2]Max Planck Institute for Solar System Research, 2 Max Planck-Strasse, Katlenburg-Lindau 37191, Germany. [3]Marshall Space Flight Center, Huntsville, Alabama 35812, USA. [4]University of Maryland, Institute for Physical Science & Technology, College Park, Maryland 20742, USA. [5]Skobeltsyn Institute of Nuclear Physics, Moscow State University, Leninskie gory, GSP1, Moscow 119991, Russia. [6]Louisiana State University, Department of Physics and Astronomy, Baton Rouge, Louisiana 70803, USA.

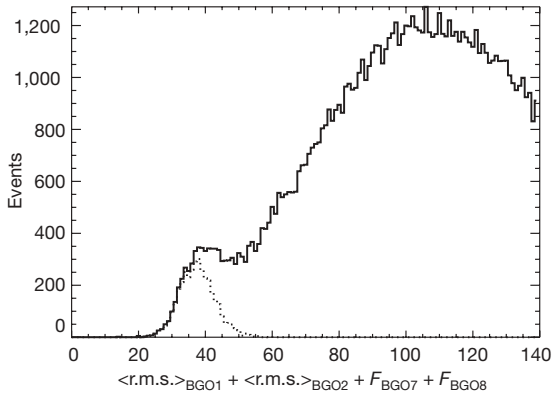

Figure 1 | Separation of electrons from protons in the ATIC instrument. Candidate electron events (162,000) with energy over 50 GeV are plotted as a histogram with the horizontal axis showing the sum of the 'weighted energy fraction' (F values as defined below) in the last two BGO layers and the shower width (root mean squared, r.m.s.) in the first two layers. The shower width is calculated as

$$\langle \mathrm{r.m.s.} \rangle^2 = \sum_{i=1}^{n} E_i (\mathrm{X}_i - \mathrm{X}_c)^2 / \sum_{i=1}^{n} E_i$$

where X_c is the coordinate of the energy centre, X_i is the coordinate of the centre of the ith crystal and E_i is the energy deposited in the ith crystal. The F value is calculated as $F_n = (E_n/\mathrm{Sum})\ \langle \mathrm{r.m.s.} \rangle^2$ where E_n is the energy deposit in BGO layer n, Sum is the total energy deposit in all BGO layers and $\langle$r.m.s.$\rangle$ refers to layer n (ref. 12). Each event is also fitted to an electromagnetic cascade profile to estimate the starting point and the depth of the cascade maximum. An event is accepted if the cascade starts above the first BGO layer, which eliminates many protons (~75%) but passes most electrons (~90%). Next a diagonal cut in r.m.s. and F is determined for each energy bin and used to isolate the electrons. This removes most of the protons (2 in 10^4 remain) and retains 84% of the electrons[12]. The selected electrons are shown as the dotted histogram.

depart from the calculated curve. They show an excess electron flux up to about 650 GeV, above which the spectrum drops rapidly, with a return to the 'general' spectrum line at ~800 GeV. In particular, over the energy range 300 to 800 GeV we observe 210 electrons, whereas GALPROP predicts only 140 events, an excess of about six standard deviations. Using a source-on/source-off method for determining 'significance'[15], we obtain an excess of roughly four standard deviations (Supplementary Information section 4).

Data recently became available from the Polar Patrol Balloon (Antarctic) flight of the BETS detector. Although of lower statistical precision, results from the PPB-BETS calorimeter[16] also indicate a possible structure and agree with the ATIC results (see Fig. 3), giving added confidence to the conclusion that this feature is real.

We varied the source injection parameters in the GALPROP code to try to reproduce the data points at 500 to 700 GeV. This required a hard injection spectrum which could not reproduce the drop in flux above 650 GeV and led to overproducing electrons above 1 TeV by a factor of almost three (and underproducing the well-measured data below 100 GeV).

The observed electron 'feature' therefore indicates a nearby source of high-energy electrons. This may be the result of an astrophysical object, as energetic electrons have been observed in a variety of astrophysical sites (for example in a supernova remnant[17], pulsar wind nebula[5,18], micro-quasar[6] or accreting intermediate-mass black hole). To fit the electron excess, such a source would need a very steep energy spectrum (spectral index around −1.4) with a high-energy cut-off at about 600–700 GeV, so as not to overproduce teraelectronvolt electrons. It is possible that a micro-quasar could produce a sharp feature in the electron spectrum[6], but such an object would need to be local (less than 1 kpc away) and active relatively recently. Imaging atmospheric Cherenkov telescopes have observed numerous

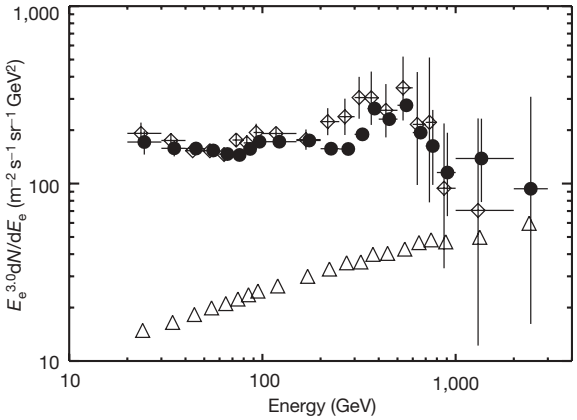

Figure 2 | ATIC-1 and ATIC-2 spectra at balloon altitude, showing good agreement with each other. The measured primary electron flux (scaled by E^3) at flight altitude is shown for ATIC-1 (open squares) and ATIC-2 (filled circles). The errors are one standard deviation. Both balloon flights were from McMurdo, Antarctica, and circumnavigated that continent. ATIC-1 was a test flight in 2000–01 and the usable data correspond to an exposure of 0.61 m^2 sr days. ATIC-2 was a science flight in 2002–03 with an exposure of 2.47 m^2 sr days. To eliminate edge effects, we restrict the incident zenith angle to be less than ~37° ($\cos\theta \geq 0.8$), use only the central 80% of the SiM and eliminate events in the outer crystals in each BGO layer. Within these limits, the electron detection efficiency above 60 GeV is 84% essentially independent of energy. The effective acceptance was determined as a function of particle energy considering the trigger efficiency, trajectory reconstruction efficiency and the geometrical restrictions. The effective acceptance of the instrument increases from 0.075 m^2 sr at 20 GeV to 0.15 m^2 sr for $E > 60$ GeV. Above 100 GeV, a total of 1,724 electron events were observed, with the highest energy event at 2.3 TeV. The total background is also shown in the figure as the open triangles and is a combination of unresolved protons, unidentified γ-rays and atmospheric secondary electrons produced in the material (~4.5 g cm^{-2}) above the instrument. ATIC becomes background limited for electrons only above several teraelectronvolts.

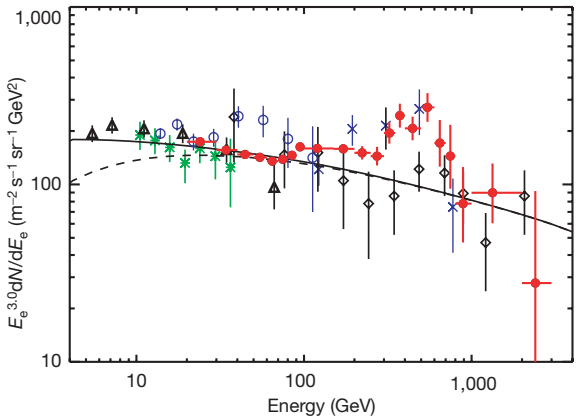

Figure 3 | ATIC results showing agreement with previous data at lower energy and with the imaging calorimeter PPB-BETS at higher energy. The electron differential energy spectrum measured by ATIC (scaled by E^3) at the top of the atmosphere (red filled circles) is compared with previous observations from the Alpha Magnetic Spectrometer AMS (green stars)[31], HEAT (open black triangles)[30], BETS (open blue circles)[32], PPB-BETS (blue crosses)[16] and emulsion chambers (black open diamonds)[4,8,9], with uncertainties of one standard deviation. The GALPROP code calculates a power-law spectral index of −3.2 in the low-energy region (solid curve)[14]. (The dashed curve is the solar modulated electron spectrum and shows that modulation is unimportant above ~20 GeV.) From several hundred to ~800 GeV, ATIC observes an 'enhancement' in the electron intensity over the GALPROP curve. Above 800 GeV, the ATIC data returns to the solid line. The PPB-BETS data also seem to indicate an enhancement and, as discussed in Supplementary Information section 3, within the uncertainties the emulsion chamber results are not in conflict with the ATIC data.

sources of high-energy gamma radiation, including pulsar wind nebula and supernova remnants, finding spectra that fall as E^{-2} with an exponential cut-off in the teraelectronvolt region[3,17]. This implies that particles have been accelerated to tens of teraelectronvolts or higher, which would not be consistent with the current electron data. The nearby object that comes closest to meeting the source requirements is the Geminga pulsar and associated remnant, whose potential contribution to high-energy electrons has been modelled[4,18]. However, the calculated flux from Geminga is about a factor of 60 too low to explain the observations (see Supplementary Information section 5). Nevertheless, the classes of object discussed here have the potential to produce energetic electrons, and there may well be a nearby, unstudied astrophysical object that is accelerating the electrons observed by ATIC.

An alternative explanation invokes annihilation of dark matter particles. There has been considerable theoretical work on the predicted dark matter distribution in the Galaxy as well as on the production and propagation of the products of dark matter annihilations[19–23]. Electrons and positrons are predicted as products of the annihilation of some exotic particles suggested as dark matter candidates[24], including weakly interacting particles from supersymmetric theories, such as neutralinos, and particles resulting from theories involving compactified extra dimensions—the 'Kaluza–Klein' (KK) particles[7]. The annihilation of supersymmetric and Kaluza–Klein types of dark matter can proceed through different channels including production of either electron–positron pairs or high-energy γ-rays (Supplementary Information section 6). The signature of this annihilation process is an increase in electron intensity above that expected from astrophysical sources, the details of which depend on the dark matter type and primary annihilation channel. Direct production of e^+e^- pairs is suppressed for supersymmetric particles, resulting in a source spectrum that has a broad peak and decreases in flux up to the particle mass[19]. This spectrum is further broadened by propagation and would not be consistent with the electron data. In contrast, direct production of e^+e^- pairs is not suppressed for Kaluza–Klein particles, resulting in a source spectrum that is dominated by a delta function at the particle mass. Energy losses during propagation broaden this distribution to lower energies. According to current theory, the mass of the lightest Kaluza–Klein particle is expected to be greater than 300 GeV (refs 19, 20). Further, the Wilkinson Microwave Anisotropy Probe (WMAP) has observed an excess in the microwave emission around the inner region of our Galaxy ('WMAP haze') that could be a product of dark matter annihilation. This assumption provides a constraint on the dark matter annihilation rate[19,23]. For Kaluza–Klein particles, the annihilation rate is inversely proportional to the square of the particle mass, and the mass of the lightest Kaluza–Klein particle that could reproduce the WMAP haze is estimated to be 550 to 650 GeV (refs 25, 26).

The GALPROP code includes the capability to inject and propagate a source of electrons resulting from the annihilation of a dark matter particle[14,21]. As an example, the spectrum produced for a Kaluza–Klein particle mass of 620 GeV is shown in Fig. 4. When added to the general spectrum, this reproduces the observed data well. The ATIC energy range includes this mass and, therefore, the calculation should be relatively immune to uncertainties in the overall dark matter distribution, and to galactic propagation, but would be sensitive to conditions in our local galactic neighbourhood[22]. The difficulty is that a model with a smooth distribution of Kaluza–Klein particles annihilating in our Galaxy produces a much smaller signal than the feature reported here. To be consistent with the WMAP haze, the annihilation rate for a 620-GeV thermal relic Kaluza–Klein particle would need to be about $4.4 \times 10^{-26}\,\mathrm{cm^3\,s^{-1}}$, a factor of ~200 smaller than that required to fit the observed electron excess. Such enhancements are usually attributed to a 'boost factor' associated with non-uniform clumps in the dark matter distribution[27], and such clumps could also be located near our Solar System[28]. Moreover, 'minispikes' of dark matter overdensities, associated for instance with intermediate-mass black holes, can result in boost factors of a few thousand[29]. In any case, the exact level of 'boost' is still subject to debate.

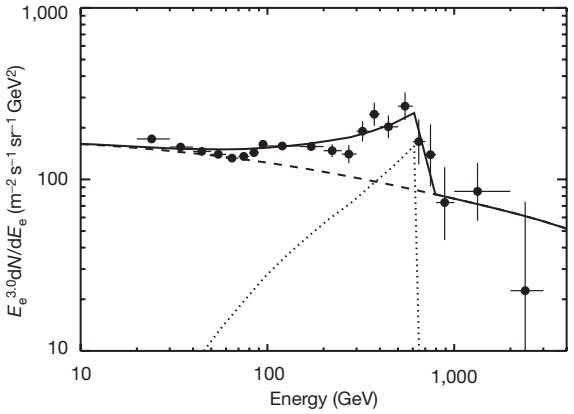

Figure 4 | Assuming an annihilation signature of Kaluza–Klein dark matter, all the data can be reproduced. The GALPROP general electron spectrum resulting from sources across the galaxy is shown as the dashed line. The dotted curve represents the propagated electrons from the annihilation of a Kaluza–Klein particle. The dotted curve assumes an isothermal dark matter halo of 4-kpc scale height, a local dark matter density of 0.43 GeV cm^{-3}, a Kaluza–Klein mass of 620 GeV, and an annihilation cross section rate of $1 \times 10^{-23}\,\mathrm{cm^3\,s^{-1}}$, which implies a boost factor of ~200. The sum of these signals is the solid curve. Here the spectrum is multiplied by $E^{3.0}$ for clarity. The solid curve provides a good fit to both the magnetic spectrometer data[30,31] and calorimeter data[16,32] and reproduces all of the measurements from 20 GeV to 2 TeV, including the cut-off in the observed excess. All error bars are one standard deviation.

It should be noted that other authors[19,21] have found the need to introduce boost factors of 200–300 to explain the cosmic-ray positron excess observed by the HEAT magnetic spectrometer experiment[30] in terms of an annihilation signature of Kaluza–Klein dark matter. Thus, a model for Kaluza–Klein dark matter annihilation that would explain the observed ATIC electron excess could also fit the excess positrons observed by HEAT at ~30 GeV.

The 'feature' in the spectrum of high-energy cosmic-ray electrons reported here provides an intriguing puzzle. Either an as yet unknown astrophysical source or the annihilation of a dark matter particle is a possible explanation. If the 'feature' is caused by an astrophysical object this would be the first direct observation of a nearby source of particles with energies of hundreds of gigaelectronvolts and would open a new window for studying such objects. Kaluza–Klein dark matter arises from multi-dimensional theories of our Universe in which the extra dimensions are 'compact', meaning that they have only a small (but non-zero) effect on our four-dimensional physical reality. If the Kaluza–Klein annihilation explanation proves to be correct, this will necessitate a fuller investigation of such multi-dimensional spaces, with potentially important implications for our understanding of the Universe.

Received 23 May; accepted 1 October 2008.

1. Tang, K.-K. The energy spectrum of electrons and cosmic-ray confinement. A new measurement and its interpretation. *Astrophys. J.* **278**, 881–892 (1984).
2. Allen, G. E. *et al.* Evidence of X-ray synchrotron emission from electrons accelerated to 40 TeV in the supernova remnant Cassiopeia A. *Astrophys. J.* **487**, L97–L100 (1997).
3. Aharonian, F. A. *et al.* High-energy particle acceleration in the shell of a supernova remnant. *Nature* **432**, 75–77 (2004).
4. Kobayashi, T. *et al.* The most likely sources of high-energy cosmic-ray electrons in supernova remnants. *Astrophys. J.* **601**, 340–351 (2004).
5. Aharonian, F. A. *et al.* Cosmic ray positrons connected with galactic gamma radiation of high and very high energies. *J. Phys. G Nucl. Part. Phys.* **17**, 1769–1778 (1991).
6. Heinz, S. & Sunyaev, R. Cosmic rays from microquasars: A narrow component in the CR spectrum. *Astron. Astrophys.* **390**, 751–766 (2002).

7. Cheng, H. C., Feng, J. L. & Matchev, K. T. Kaluza–Klein dark matter. *Phys. Rev. Lett.* **89,** 211301 (2002).
8. Nishimura, J. *et al.* in *25th ICR Conf. Papers* Vol. 4 (eds Potgieter, M. S., Raubenheimer, B. C. & van der Walt, O. J.) 233–237 (Space Research Unit, Durban, 1997).
9. Nishimura, J. *et al.* Emulsion chamber observations of primary cosmic-ray electrons in the energy range 30–1000 GeV. *Astrophys. J.* **238,** 394–409 (1980).
10. Guzik, T. G. *et al.* The ATIC long duration balloon project. *Adv. Space Res.* **33,** 1763–1770 (2004).
11. Ganel, O. *et al.* Beam tests of the balloon-borne ATIC experiment. *Nucl. Instrum. Methods A* **552,** 409–419 (2005).
12. Chang, J. *et al.* Resolving electrons from protons in ATIC. *Adv. Space Res.* **42,** 431–436 (2008).
13. Chang, J. *et al.* in *Proc. 28th Intl Cosmic Ray Conf.* (eds Kajita, T., Asaoka, Y., Kawachi, A., Matsubara, Y. & Sasaki, M.) 1817–1820 (Universal Acad. Press, Tokyo, 2003).
14. Strong, A. W. & Moskalenko, I. V. Models for galactic cosmic-ray propagation. *Adv. Space Res.* **27,** 717–726 (2001).
15. Li, T. P. & Ma, Y.-Q. Analysis methods for results in gamma-ray astronomy. *Astrophys. J.* **272,** 317–324 (1983).
16. Torii, S. *et al.* High energy electron observation by Polar Patrol Balloon flight in Antarctica. *Adv. Polar Upper Atmos. Res.* **20,** 52–62 (2006).
17. Aharonian, F. A. *et al.* Very high energy gamma rays from the composite SNR G 0.9+0.1. *Astron. Astrophys.* **432,** L25–L29 (2005).
18. Büsching, I., de Jager, O. C., Potgieter, M. S. & Venter, C. A cosmic-ray positron anisotropy due to two middle-aged, nearby pulsars? *Astrophys. J.* **678,** L39–L42 (2008).
19. Hooper, D. & Silk, J. Searching for dark matter with future cosmic positron experiments. *Phys. Rev. D* **71,** 083503 (2005).
20. Applequist, T. & Yee, H.-U. Universal extra dimensions and the Higgs boson mass. *Phys. Rev. D* **67,** 055002 (2003).
21. Moskalenko, I. V. & Strong, A. W. Galactic propagation of positrons from particle dark-matter annihilation. *Phys. Rev. D* **60,** 063003 (1999).
22. Delahaye, T. *et al.* Positrons from dark matter annihilation in the galactic halo: Theoretical uncertainties. *Phys. Rev. D* **77,** 063527 (2008).
23. Hooper, D. Indirect searches for dark matter. Preprint at ⟨http://arXiv.org/abs/0710.2062v1⟩ (2008).
24. Drees, M. & Gerbier, G. Supersymmetric dark matter. *Phys. Lett. B* **592,** 216–219 (2004).
25. Servant, G. & Tait, T. M. P. Is the lightest Kaluza–Klein particle a viable dark matter candidate? *Nucl. Phys. B* **650,** 391–419 (2003).
26. Hooper, D., Finkbeiner, D. P. & Dobler, G. Possible evidence for dark matter annihilation from excess microwave emission around the center of the Galaxy seen by the Wilkinson Microwave Anisotropy Probe. *Phys. Rev. D* **76,** 083012 (2007).
27. Lavalle, J. *et al.* Full calculation of clumpiness boost factors for antimatter cosmic rays in the light of ΛCDM *N*-body simulation results: Abandoning hope in clumpiness enhancement? *Astron. Astrophys.* **479,** 427–452 (2008).
28. Diemand, J. *et al.* Clumps and streams in the local dark matter distribution. *Nature* **454,** 735–738 (2008).
29. Brun, P. *et al.* Antiproton and positron signal enhancement in dark matter minispikes scenarios. *Phys. Rev. D* **76,** 083506 (2007).
30. Barwick, S. W. *et al.* Measurements of the cosmic-ray positron fraction from 1 to 50 GeV. *Astrophys. J.* **482,** L191–L194 (1997).
31. Alcaraz, J. *et al.* Leptons in near Earth orbit. *Phys. Lett. B* **484,** 10–22 (2000).
32. Torii, S. *et al.* The energy spectrum of cosmic-ray electrons from 10 to 100 GeV observed with a highly granulated imaging calorimeter. *Astrophys. J.* **559,** 973–984 (2001).

Supplementary Information is linked to the online version of the paper at www.nature.com/nature.

Acknowledgements This research was supported in the USA by NASA, in Russia by the Russian Foundation for Basic Research, and in China by the National Natural Science Foundation. The help of the NASA BPO and CSBF during balloon flights and the US NSF and RPSC for Antarctica operations is gratefully acknowledged.

Author Contributions Each institution in the ATIC collaboration assumed particular roles, each of which provided important contributions to this paper. In particular, the Max Planck Institute and Purple Mountain Observatory (PMO) developed the electron observation techniques. Marshall Space Flight Center (MSFC), Moscow State University (MSU) and Louisiana State University (LSU) developed the hardware which was integrated at LSU, who also led the flight team. The University of Maryland (UMD) and MSU performed instrument simulations and processed the data. PMO led the electron analysis of the flight data and LSU and PMO prepared the manuscript.

Author Information Reprints and permissions information is available at www.nature.com/reprints. Correspondence and requests for materials should be addressed to J.P.W. (wefel@phunds.phys.lsu.edu).